IRANIAN JOURNAL OF CATALYSIS

Fluidized bed photoreactor for the removal of acetaminophen and pyridine using Al-doped TiO_2 supported on alumina

Carlos Montalvo*[a], Ruby Sheila Gines[b], Denis Cantu[b], Alejandro Ruiz[a], Claudia Alejandra Aguilar[a], Isai Perez[a], Rosa Maria Ceron[a]

a) Faculty of Chemistry, Autonomous University of Carmen, Carmen City, Campeche, México.
b) Orizaba Technological Institute, Division of Graduate Studies and Research. Orizaba, Veracruz, México.

Received 23 November 2021; received in revised form 22 June 2022; accepted 18 July 2022 (**DOI: 10.30495/IJC.2022.1945335.1893**)

ABSTRACT

In this investigation, a fluidized bed photocatalytic reaction system was designed to eliminate emerging contaminants: acetaminophen and pyridine in water. Titanium dioxide (TiO_2) doped with aluminum (Al^{3+}) using the photo-deposition technique was used as a catalyst and supported on alumina beads (Al_2O_3). The catalyst´s doping was carried out by photo deposition with aluminum particles. The reactor, which is a quartz vessel with a capacity of 500 mL, where aluminum pearl, was previously impregnated with titanium oxide and calcined at 550 °C. The reactor feeding was carried out using a pump at a flow of 0.5 L/min; two lamps of UV light with 365 nm were used. The synthesized catalyst was characterized through Energy-dispersive X-ray analysis (EDX), Transmission Electron Microscopy (TEM), and X-ray diffraction (XRD) techniques, showing adequate impregnation of aluminum in the formed compound. Photoactivity analysis of the catalyst was performed at different contaminant concentrations, from 5-40 ppm for acetaminophen and 5-60 ppm for pyridine. Mineralization of more than 85% acetaminophen and 70 % pyridine was achieved after 300 min of UV illumination. The results demonstrate that using this photocatalytic arrangement as a decontamination technique for the pollutants such as acetaminophen and pyridine is feasible.

***Keywords**: Photodegradatio; fluidized bed reactor; pyridine; acetaminophen*

1. Introduction

Water pollution is an issue worldwide of vital importance because many aromatic compounds are being discharged as pollutants into the environment [1]. Among these discharged aromatic compounds, acetaminophen and pyridine are the most used and most dangerous chemical contaminants of water sources, as they have toxicological effects on humans, animals, and plants [2]. Paracetamol, known as acetaminophen with the chemical formula $C_8H_9NO_2$, is a heterocyclic compound belonging to amides [3]. A white powder dissolved in water has a transparent color with a density of 1263 g/cm^3, a melting point of 169 °C, and a boiling point of more than 500 °C. Acetaminophen is an active ingredient in hundreds of drugs used to relieve pain and fever; if used more than indicated, it can cause severe hepatic damage and gastrointestinal complications in humans [4]. Acetaminophen is a toxic compound, which is present exclusively in aquatic environments [5] and persistent in wastewater treatment plants. Marine organisms inhibit acetylcholinesterase activity, neurotoxicity, and clams cause necrosis and cell death [6].

On the other hand, pyridine is a basic heterocyclic compound with the chemical formula C_5H_5N; it is a colorless compound with a boiling point of 115.2 °C and a melting point of 41.6 °C, and a density of 0.9819 g/cm^3 [7]. Pyridine is used as a solvent in the paint and rubber industry and also to manufacture insecticides and herbicides; it is also used to formulate medicines, vitamins, dyes, and adhesives [1, 2]. Clinical studies of human exposure have provided some information on pyridine, mainly related to medical treatments or exposure to its vapors; it is absorbed through the digestive, cutaneous, or respiratory route; the clinical

*Corresponding author:
E-mail address: c_montalvo10@hotmail.com and cmontalvo@pampano.unacar.mx
(**C. Montalvo**)

symptoms of intoxication consist of gastrointestinal disturbances, diarrhea, abdominal pain, nausea, weakness, headache, insomnia, and nervousness. Exposure to concentrations below those required to produce overt clinical signs may cause liver injury of varying degrees, with severe central lobe degeneration, congestion, and cellular infiltration. Repeated exposures to low concentrations of pyridine cause cirrhosis. The kidney appears less sensitive than the liver. Pyridine and its derivatives generally produce local irritation when they meet the skin, mucous membranes, and cornea. Liver damage can occur from exposure to too small concentrations to elicit a nervous system response, therefore, exposed users may not always be aware of the presence of this substance.

Furthermore, although the odor of pyridine is easily detected at vapor concentrations below one ppm, the sense of smell cannot be relied upon because it quickly becomes numb. Pyridine is a liquid and gaseous state that becomes a severe fire and explosion hazard when exposed to flame; it can also react violently with oxidizing substances. If Pyridine is decomposed by heat, it gives off cyanide vapors [8]. Contact with pyridine can cause damage to the liver, kidneys, immune system, and reproductive functions in the human body. In wastewater, pyridine concentration can vary between 20-300 mg/L when the maximum allowable limit is 1 mg/L [9].

Acetaminophen and pyridine are recalcitrant organic compounds, and their treatment represents a challenge because physical and chemical methods are expensive, and conventional biological treatments are often inefficient [10]. In recent years, acetaminophen has been one of many countries' most consumed pharmaceutical products. In 2009, 54.3 g and 22.6 g of acetaminophen/habitant per year were reported in France and Spain. After consumption, it is excreted in native and metabolized forms into sewage systems, reaching sewage treatment plants and other aquatic environments [11]. The advanced oxidation processes (AOPs), which are characterized by the production of the powerful oxidizing species ·OH radicals, are considered efficient in decomposing recalcitrant substances such as pyridine and acetaminophen. Heterogeneous photocatalysis is based on the generation of hydroxyl radicals using oxidation-reduction reactions that occur on the surface of a photocatalyst due to the action of UV light and the presence of oxygen as an oxidizing agent. In the interfacial region, pollutant destruction reactions occur without the photocatalyst undergoing chemical changes. The photocatalyst can be in the form of a suspension to increase the area of action or immobilized on some support to avoid a subsequent separation step and additionally to allow its reuse [13].

TiO_2 is the most widely used heterogeneous semiconductor photocatalysis [14] due to its high photoactivity, chemical stability, and low cost, which makes it an excellent candidate for photocatalytic reactions due to its relatively large, prohibited band (3.0-3.2 eV) and the ability to absorb ultraviolet light [15]. Recent research has focused on evaluating changes in their properties when making structure modifications doped with another metal [16] to improve its photocatalytic capacity.

The photocatalytic reaction in semiconductors begins when a photocatalyst adsorbs a photon of energy equal to or greater than the energy value of its band gad. When this occurs, an electron is promoted from the valence band to the conduction band, generating a vacancy of electrons or holes in the valence band. By maintaining the separation of charges, the hole (h^+) and the electron (e^-) can migrate to the surface of the catalyst, where they participate in oxidation and reduction reactions, respectively, with the species adsorbed there [17]. The photo-generated voids have a positive charge and can oxidize water molecules or hydroxyl ions adsorbed on the catalyst surface, thereby generating highly oxidizing species (equations 1 and 2):

$$h^+ + H_2O_{(ads)} \leftrightarrow H_2O^+_{(ads)} \leftrightarrow \cdot OH_{(ads)} + H^+ \quad (1)$$

$$h^+ + OH^-_{(ads)} \leftrightarrow \cdot OH_{(ads)} \quad (2)$$

The activated hydroxyl radicals (·OH) formed from such reactions act as strong nucleophiles and are capable of breaking molecular structures with high electron density, such as aromatic rings or unsaturated aliphatic chains. On the other hand, the photo-generated electrons in the semiconductor´s conduction band react with the adsorbed oxygen molecules to produce the superoxide radical ($O\cdot_2^-$), as shown in equation 3. These radicals are rapidly converted into hydrogen peroxide and subsequently activated hydroxyl radicals. Both radicals can oxidize nearby chemical species and, in the case of organic molecules, mineralize to CO_2 and H_2O.

$$e^- + O_{2(ads)} \leftrightarrow O\cdot_2^-{}_{(ads)} \quad (3)$$

$$O_{2(ads)} + 2H^+ \leftrightarrow H_2O_{2(ads)} \quad (4)$$

$$e^- + H_2O_{2(ads)} \leftrightarrow \cdot OH_{(ads)} + OH^-_{(ads)} \quad (5)$$

The efficiency of these reactions depends on four processes: the adsorption of light by the semiconductor, the separation of the electron-hole pair, the migration of the photogenerated pairs towards the catalyst´s surface, and the rate of recombination of the photogenerated pairs. The recombination of the photogenerated pairs

can be retarded by metal ions such as Cu^{2+} and can also serve as charge trapping sites and thus decrease the electron. In addition, the effect of doping on activity depends on many factors, including the doping method and the type and concentration of dopant elements. Doping metallic and non-metallic elements are considered a promising approach to improving the photocatalytic efficiency of TiO_2. Noble metals are known to exhibit well-defined surface plasmon resonance (LSPR) properties suitable for various applications, such as photocatalysis. The synthesis of plasmonic photocatalysts shows high photoactivity for removing organic pollutants at different wavelengths [19, 20]. However, the wide practical applications of noble metal-based nanostructures are impeded by their high price, significant optical losses, and limited wavelength range. Recently, researchers have broadened the scope of these applications by investigating alternative LSPR materials such as non-noble metals, including aluminum [21]. Aluminum is a relatively inexpensive metal, easy to fabricate, with an electronic structure that allows it to maintain a more flexible optical performance than other metals (Cu, Au, or Ag), with a wavelength range extending over the entire UV-Vis-IR spectrum [22, 23].

To enhance the photocatalytic activity of Al-TiO_2, the incorporation of adsorbent material is very important. Activated alumina is a material frequently used to remove pollutants in water, as it is attributed with adsorption properties [24]. The solid-porous supported catalyst should be granular in shape; so that it can be easily filtered from the treated water and reused. Because the active phase TiO_2 is dispersed on porous support with a very high surface area, the photocatalytic activity of the supported TiO_2 can be considerably higher than that of powdered TiO_2 particles [25]. The present study aims to investigate the photocatalytic degradation of pyridine and acetaminophen. This reagent is extensively used in industry, in a fluidized bed photoreactor, in the presence of TiO_2 doped with Al^{3+} and supported on Al_3O_2 beads. The supported catalyst was characterized by techniques such as TEM, XRD, and EDX. Photocatalytic degradation of the organic compounds was monitored by a combination of analytical techniques such as UV-Vis spectroscopy and HPLC. The kinetic parameters of the Langmuir-Hinshelwood model that describe the initial reaction rate for the photocatalytic degradation of acetaminophen and pyridine in a fluidized bed photoreactor are presented.

2. Experimental

2.1 Chemicals products and reagents

The reagents used to carry out the synthesis of the catalyst are aluminum sulfate (Al_2 $(SO_4)_3$) purchased from Sigma-Aldrich, Alumina (Al_2O_3) in beads acquired by Dese Camen, and Titanium Dioxide (TiO_2) Degussa P25. The photoactivity of the catalyst was evaluated by: Acetaminophen ($C_8H_9NO_2$) obtained from Sigma-Aldrich, pyridine (C_5H_5N) purchased from Sigma-Aldrich, and distilled water purchased from Fermont. All chemicals were of analytical reagent grade.

2.2 Preparation of Al-TiO_2/ Al_2O_3

For the impregnation of the semiconductor TiO_2 in the activated alumina beads, the wet impregnation technique was used, for which a solution of 3.5 g of titanium dioxide was prepared in 300 mL of distilled water in which the alumina beads were immersed, gently stirred for 30 minutes, and allowed to stand for 24 hours to achieve maximum adsorption of the semiconductor in the activated alumina beads. The residue was removed from the titanium dioxide solution; the beads were distributed into porcelain vessels and placed in the flask at 550 °C for 2 hours.

For aluminum doping, the photo-deposition method was used, a solution of 400 ppm of aluminum sulfate precursor salts Al_2 $(SO_4)_3$ was prepared, and the beads with the titanium oxide coating were placed in the reactor, and the aluminum sulfate solution was recirculated. Initially, the solution was recirculated for 1 hour in the dark phase for maximum adsorption followed by a further 5 hours with the irradiation of the 365 nm 4 UV light lamps [26].

After the 6-hour reaction period, recirculation of the solution was stopped to remove the excess solution from the reactor. Finally, the beads were allowed to stand for one day and were calcined at a temperature of 550 °C for 1 h.

2.3 Catalyst Characterization

photocatalyst was characterized by X-Ray Diffraction (XRD) using Rigaku equipment, model SMART LAB, and as an X-ray source, a copper tube; to determine the chemical phases and crystallographic properties of the synthesized material [27]. In most processes, the effective use of nanocatalysts depends on the size of the particles and the ease of handling them. Therefore, it is of vital importance to characterize them by using effective methods at a low cost [28]. Transmission Electron Microscopy (TEM) is a technique by which it is possible to conclude whether the synthesis of the catalyst and the dopant agent has been successful [29], for which a Tecnai F20 Super Twin TMP transmission

electron microscope from FEI was used. Finally, to provide mappings of the quantified elements of the sample; Energy Dispersive Spectroscopy (EDS) using a Tecnai F20 Super Twin TMP transmission electron microscope from FEI El was used. This analysis analysis provides information on the elemental composition of the sample providing the percentages of the TiO_2 catalyst on the support, as well as the presence of aluminum metal ions. To estimate the band gad value (Eg), the catalysts were analyzed by UV spectroscopy using a Shimadzu system, model UV-2450, equipped with the ISR-2200 Integrating Sphere Attachment.

2.4 Design and construction of the fluidized bed photoreactor

The fluidized bed reaction system was designed and constructed to degrade organic pollutants at the laboratory level. The photoreactor consists of a stainless-steel annular cylinder in which there are four15 W ultraviolet light lamps with a wavelength of 365 nm. In the unit's center, there is a reaction cell where the alumina beads with the impregnated catalyst are placed. There is a fan at the bottom of the system to avoid temperature rise in the photoreactor, as shown in **Fig. 1**.

2.5 Photodegradation tests

To carry out the degradation runs of contaminants (acetaminophen and pyridine), different solutions were prepared at different concentrations: 5,10, 15, 20, 25, 30, 35 and 40 ppm for acetaminophen and solutions of 5, 10, 15, 20, 25, 30, 35, 40, 45, 50, 55, and 60 ppm for pyridine. The pH managed was 6.8, the natural pH of the solution. This pH is adequate in other investigations [30]. The solutions were placed in the 0.5 L capacity photoreactor for 300 minutes, and samples were taken every 30 minutes to monitor the photodegradation of the contaminants. For reaction kinetics analysis, samples were filtered with a Millipore GV membrane (pore diameter 0.22 μm, Merck, Millipore, Burlington, MA, USA).

The final solution was analyzed using High-Performance Liquid Chromatography (HPLC) on an Agilent 1100 Series equipment (Autonomous University of Carmen, Campeche, Mexico) with the following specifications: Column Zorbax ODS 4.6, 150 mm, 5 m; flow conditions: 1 mL/min, detector: UV-Vis at 242 nm; mobile phase: water-methanol (50/50).

The Langmuir-Hinshelwood (L-H) model was used as a mathematical model to determine the value of the kinetic constants of the photocatalytic process.

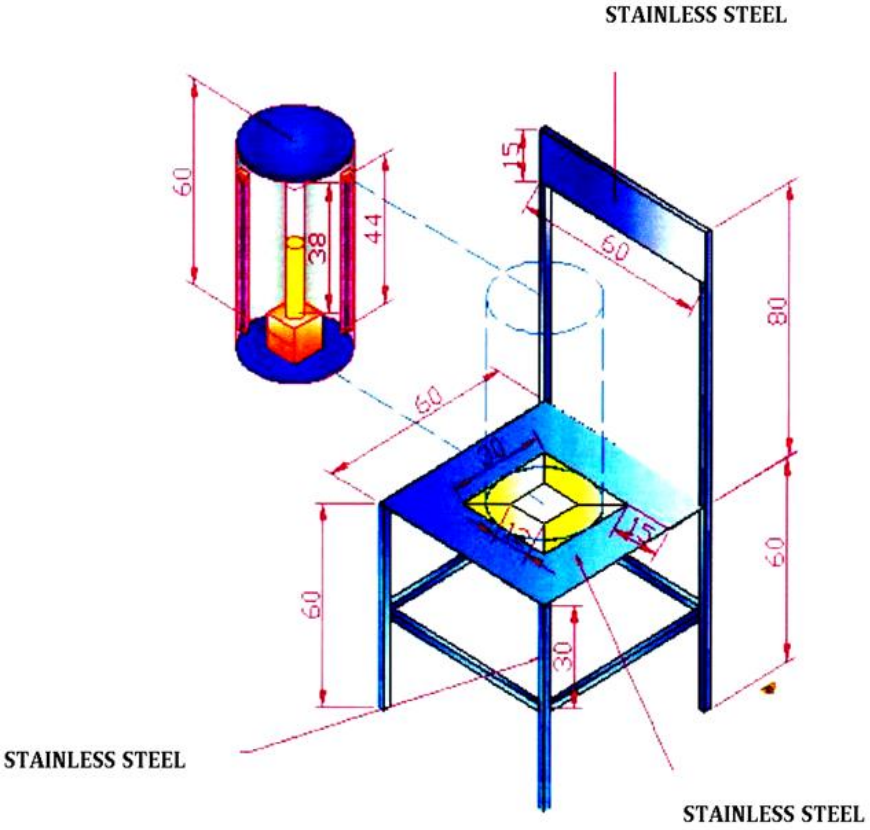

Fig. 1 Fluidized bed photoreactor

3. Results and Discussion

3.1 Catalyst Characterization

The importance of verifying the phase obtained with the synthesis method and the heat treatment applied lies in the fact that TiO_2 is a compound that presents polymorphism observed in three phases: rutile, anatase, and brookite. The three phases have different physical properties, which are essential in the application; rutile is the only stable phase. The other two are metastable and transform to rutile by heating. It has been reported that the anatase phase changes to rutile at temperatures from 400 to 1000 °C. [29].

The diffractogram of the catalyst **Fig. 2** reveals differences between TiO_2 and Al-TiO_2/ Al_2O_3. Similarly, the material calcined at 550 °C showed a high degree of crystallinity, as well as the existence of the anatase phase. When using high calcination temperatures ranging from 500 to 650 °C, neither the crystal shape nor the particle size is affected [31]. The observed diffraction pattern of TiO_2 at 2θ's (25.43), (42.3), (53.84), and (62.7) belongs to anatase. TiO_2 XRD standards are matched to JCPDS card No. 21-1272 (anataseTiO_2) In the X-ray diffraction spectrum of figure 2 B in figure A, the diffraction pattern TiO_2 doped with aluminum and supported on alumina in 2 θ (33.17, 39.8, 52 61.5 corresponds to rutile) is observed. The 2 θ peak at 39, 45, and 65 corresponds to aluminum; they are matched to the JCPDS card file no. 36-1451.

On the other hand, the particle size of the TiO_2 present in the materials was calculated using the Scherrer formula:

$$D = \frac{0.9 * \lambda}{B * Cos\ \theta}$$

Where D (nm) = crystal grain diameter, λ (nm) = wavelength of X-rays (0.154906), θ (rad) = Bragg angle, and B (rad) = width of the peak at the middle of the maximum height.

Table 1 shows the particle size of TiO_2 in the catalysts, obtained at different diffraction angles, which were chosen so that the spectra of the elements do not interfere. In these results, a slight increase in the TiO_2 particle size was observed, suggesting that this was alumina plus the added aluminum particles promoting the growth of the TiO_2 particles.

To observe the surface morphology of the catalyst, transmission electron microscopy (TEM) was used; it can be seen in **Fig. 3** that the titanium oxide presents different morphologies, where the quasi-spherical morphology predominates with a size of less than 50 nm; this is because the temperature to which it was subjected for its activation was 550 °C, the optimum temperature for the formation of the crystalline phase in anatase and rutile composition [32].

The particle size of the catalyst is homogeneous, without forming agglomerates, which facilitates its subsequent use of characterization and degradation processes [17].

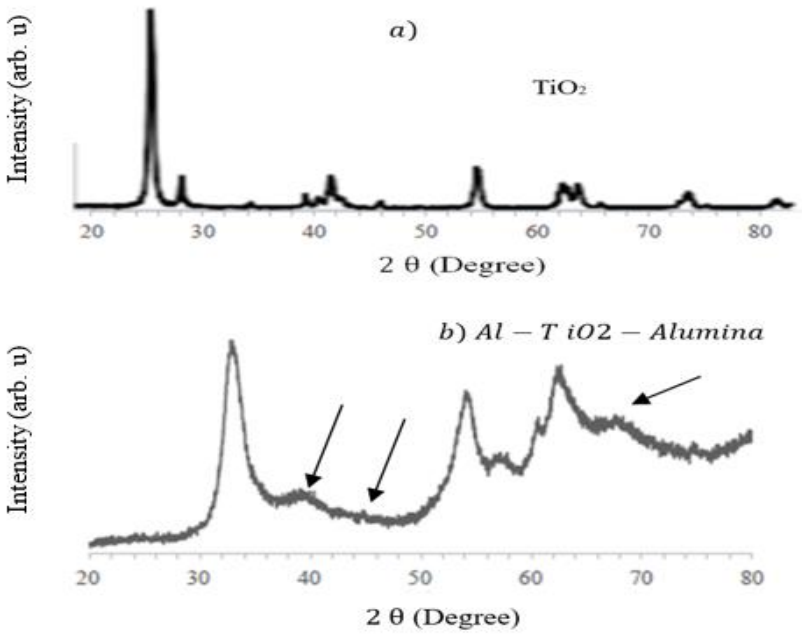

Fig. 2 X-ray diffraction patterns of a) TiO_2/ Al_2O_3 b) Al-TiO_2/ Al_2O_3 with calcined at 550 ºC

Table 1. Obtained particle size

Material	2 θ=54	2 θ=25
TiO_2	6.32	7.7
TiO_2-Al_2O_3-Al	7.6	

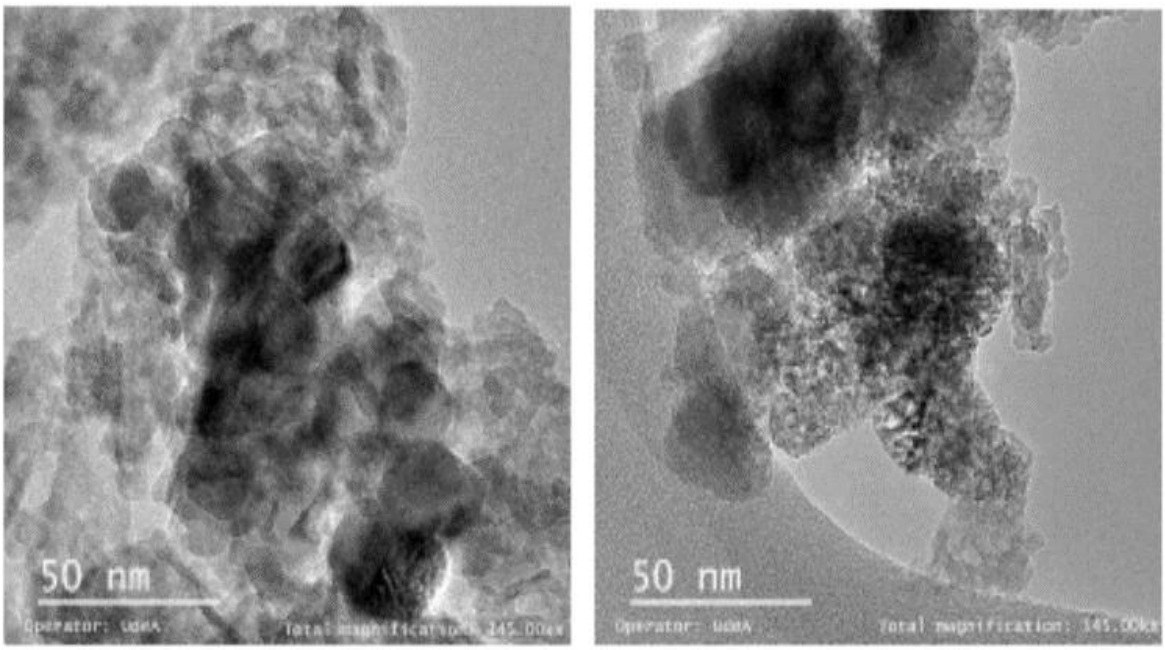

Fig. 3 Transmission Electron Microscopy (TEM) of the Al-TiO_2/ Al_2O_3 catalyst was calcined at 550 °C for 1 hour.

During the calcination, the dispersed aluminum ions gradually migrated towards the surface of TiO_2; that is to say, the metal element (Al) was deposited on the surface of the semiconductor (TiO_2), favoring the formation of a highly crystalline structure. The transfer of the electron from the titanium conduction band to the metallic aluminum particles occurs at the different Fermi energy levels between these two, which improves the photocatalytic activity of the catalyst.

Energy-dispersive X-ray analysis (EDX) was used to differentiate the sample's chemical composition. The study of the elemental composition of the catalyst sample can be seen in **Table 2**, where the percentages of the TiO_2 catalyst in the support as well as the presence of the metal ions of aluminum deposited on it are presented; this gives us a clear view of the relationship that one has with the other since, if the doping species is in excess of the catalyst, this would affect its photocatalytic performance at the time of irradiation and would not allow the passage of photons to the surface altering the activation.

In **Fig. 4a**, the results show fractions of titanium and oxygen corresponding to the semiconductor material and a higher percentage of aluminum corresponding to the support; **Fig. 4b** confirms the presence of aluminum fractions on the catalyst surface after photo-deposition by analyzing the specific particle fraction of the catalyst.

The importance of verifying the phase obtained with the synthesis method and the heat treatment applied lies in the fact that TiO_2 is a compound that presents polymorphism observed in three phases: rutile, anatase, and brookite. The three phases have different physical properties, which are essential in their application. The rutile phase is the only stable one. The other two are metastable and transform to rutile by heating. It has been reported that the anatase phase changes to rutile at temperatures from 400 to 1000 °C. For the determination of the band gap, the doped catalysts were analyzed by UV spectroscopy using a Shimadzu UV-2450 with an ISR-2200 Integrating Sphere Attachment. Measurements were taken in the range of wavelength between 200 and 600 nm.

Table 2 Elemental composition of the catalyst

Element (TiO_2/ Al_2O_3)	Weight (%)	Atomic (%)	Uncertainty (%)	Correction	K-factor
O (K)	37.55	61.50	0.14	0.51	1.889
Al (K)	10.22	9.92	0.05	0.92	1.030
Ti (K)	52.22	28.56	0.12	0.98	1.227
Element (Al-TiO_2/ Al_2O_3)	Weight (%)	Atomic (%)	Uncertainty (%)	Correction	K-factor
O (K)	45.14	58.46	0.17	0.51	1.889
Al (K)	53.08	40.76	0.13	0.92	1.030
Ti (K)	1.76	0.76	0.02	0.98	1.227

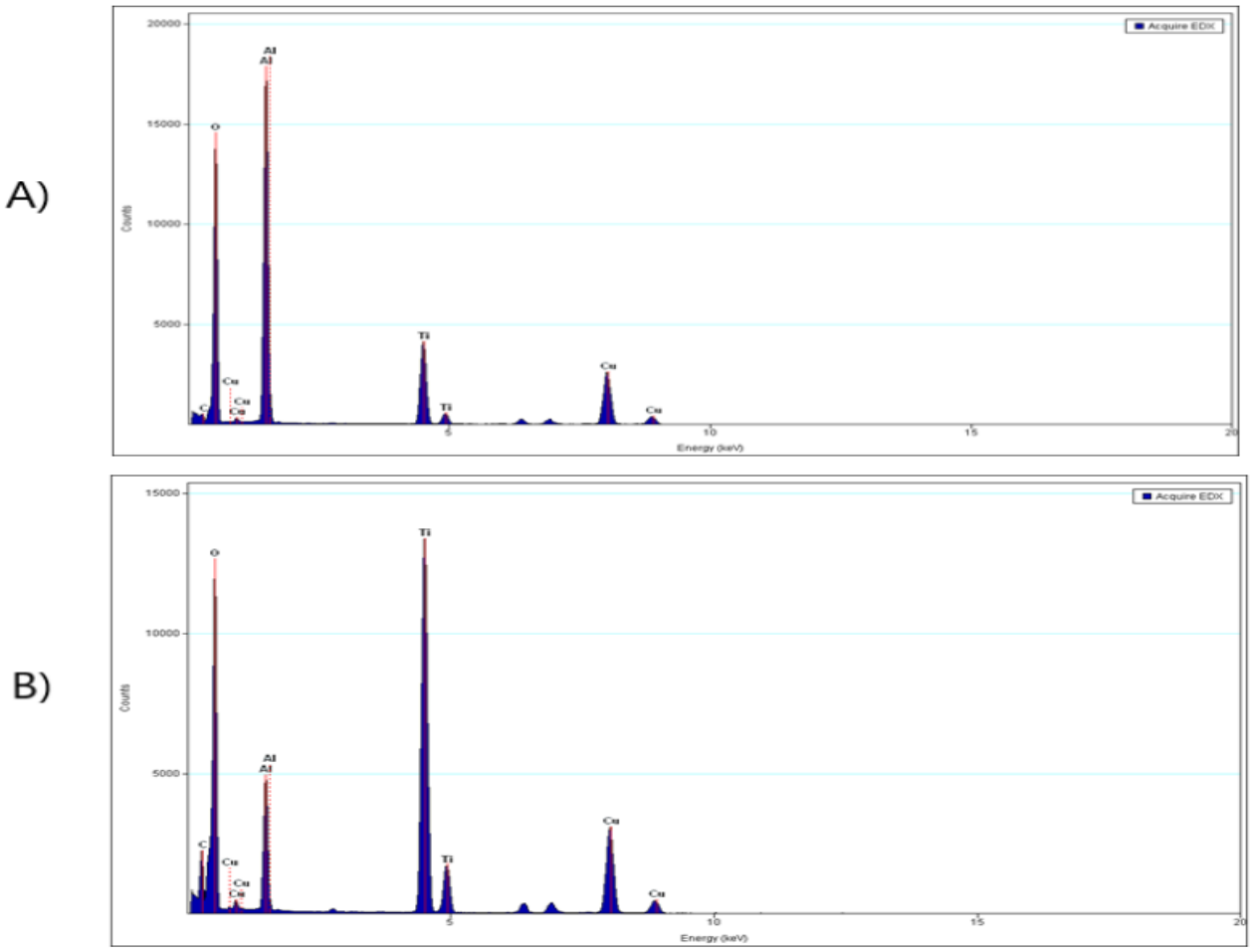

Fig. 4 Chemical composition of catalyst a) TiO_2/ Al_2O_3 y b) Al-TiO_2/ Al_2O_3. Results obtained from the analysis of retro secondary electrons (EDX)

For the calculation of the bandgap, the function of Kubelka Munk is converted according to an established procedure [33], wavelength data are transformed to frequency through the equation $\nu = \frac{c}{\lambda_g}$ and it was represented $(Abs * h\nu)^{\frac{1}{2}}$ in the function of $h\nu$, through extrapolation of a straight line toward the x-axis from the generated chart, the value of the bandgap is determined (Fig. 4)

$$E_g = \frac{hc}{\lambda_g} = \frac{h(\nu\lambda_g)}{\lambda_g} = h\nu$$

Where:

λg = Wavelength (nm)

h = Planck constant

c = Speed of light in vacuum

Figure 5 (a) compares the doped and commercial catalysts; the absorption differences in the range of 500-600 nm are attributed to aluminum particles deposited on the solid. A semiconductor experiences a charge balance when it is excited and in contact with metallic aluminum nanoparticles. This balance directly influences the Fermi energy levels by changing to more negative potentials [34], which improves the photocatalysis processes; however, according to these investigations, there is a dependence on the size of the aluminum particle deposited in the semiconductor. Likewise, the presence of metallic elements can increase the properties and electrical conductivity of a semiconductor when doped [35].

The band gap is determined from the plot between (Abs _ hv)$^{1/2}$ in the function of hv, the value of the Eg determined is the 3.1 eV for TiO_2 un-doped and Eg 2.8 eV for doped TiO_2.

According to the results obtained, the theoretical amount of aluminum particles deposited on the surface of the semiconductor had no influence on modifying the band gap compared to the un-doped catalyst.

3.2 Photo-degradation tests

Uv-Vis spectra of the degradation of the pollutants (acetaminophen and pyridine) were performed with the catalyst Al-TiO_2/Al_2O_3. The most intense absorption points were detected in the reaction samples at a wavelength of 242 nm for acetaminophen and 256 nm for pyridine, which were taken as references for the kinetic analysis of these compounds.

Fig. 6 presents the variety of the concentrations in ppm that acetaminophen undergoes when exposed to degradation by UV light and using the Al-TiO_2/Al_2O_3 catalyst in the fluidized bed reactor. It is observed that the chemical degradation of the compound is remarkable as time elapses until reaching 85% conversion of acetaminophen during 300 minutes of the photocatalytic reaction.

Fig. 7 shows the variation of the ppm concentrations of pyridine when exposed to degradation by UV light and the Al-TiO_2/ Al_2O_3 catalyst was used in the fluidized bed reactor. At the end of 300 min of the Al-TiO_2/Al_2O_3 catalyst, the degradation efficiency was 70%.

Of the two pollutants analyzed under the same operating conditions, the higher removal percentages were obtained for acetaminophen, which can be associated with the loss or detachment of the doped catalyst from the support due to its use and washing in each degradation test. The concentration of the catalyst is vital for the effective removal of pollutants because the lower concentration of the catalyst causes the efficiency of photodegradation to decrease.

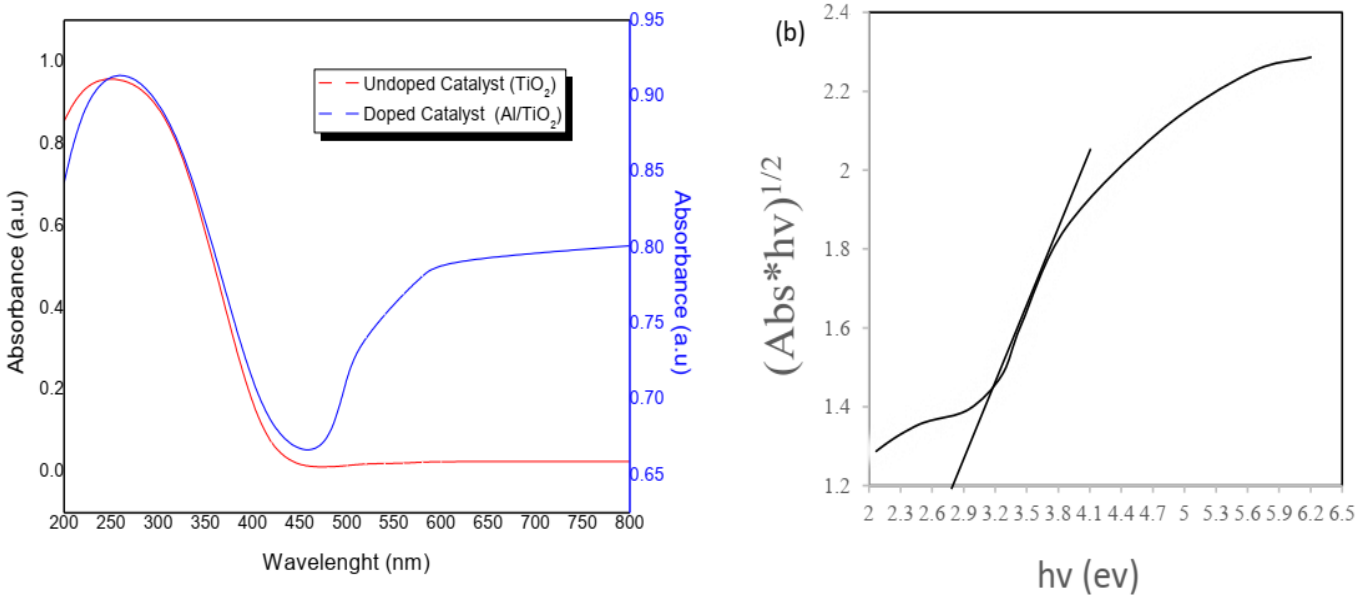

Fig. 5 (a) Kubelka Munk plots of the Al-TiO_2 catalysts and the TiO_2 P-25 catalyst. (b) Normalization of diffuse reflectance data for bandgap calculation.

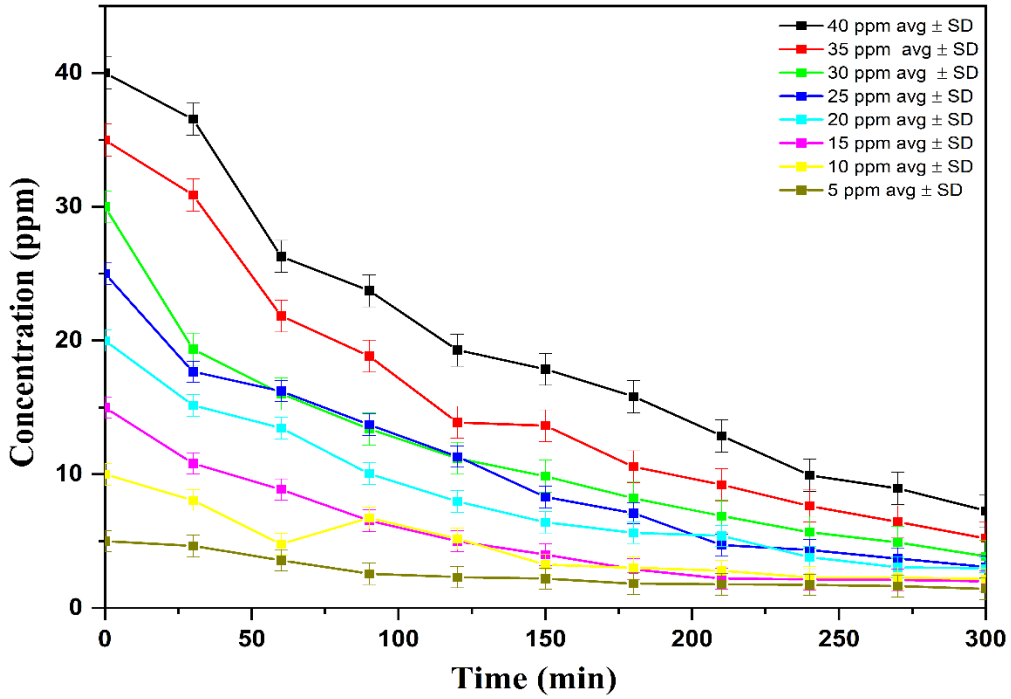

Fig. 6 Degradation of acetaminophen using as catalyst Al-TiO_2/ Al_2O_3 (catalysts dose: 11.6 g L^{-1}, photodegradation time: 300 min, pH: 6.8

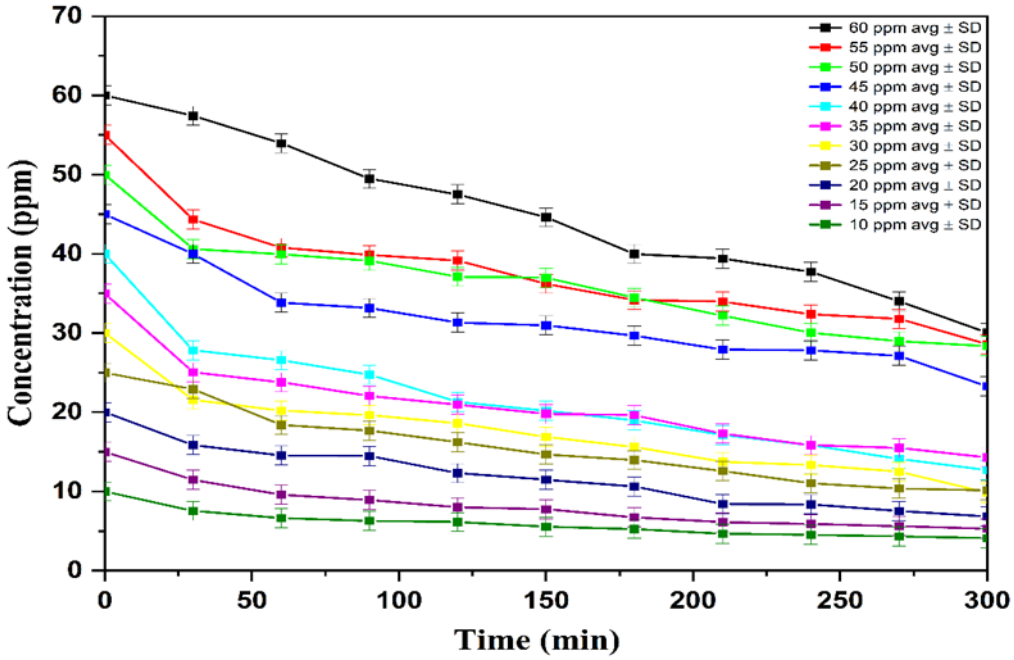

Fig. 7 Degradation of pyridine using as catalyst Al-TiO_2/ Al_2O_3 (catalysts dose: 11.6 g L^{-1}, irrad time: 300 min, pH: 6.8)

It is also important to mention that the concentration catalyst should not be excessive, which could cause the deactivation of the activated molecules due to the collision with the molecules in the basal state [36]. It affects the generation of hydroxyl radicals and the probability that the acetaminophen and pyridine molecules can react with the hydroxyl radicals [37].

The other reason for the lower percentage of pyridine removal was the concentration increase from 5-60 ppm because more pyridine molecules are adsorbed on the catalyst´s surface, resulting in decreasing the photoactive sites of the catalyst as well as the generation of hydroxyl radicals. When the initial pyridine concentration increases from 5-60 ppm, the degradation

efficiency decreases, which did not occur with the pollutant acetaminophen with concentrations from 5 to 40 ppm, obtaining higher removal percentages [38].

Changes in the slope of the removal curves of both contaminants can be observed, which may be due to intermediate compounds present in the degradation. In pyridine, the formation of ammonia, dimethylamine, formic acid, acetic acid, glutaconic acid, and oxalic acid [39] for the oxidation of acetaminophen degradation compounds are formed, such as formic acid, pyrogallol, benzene (hydroquinone, hydroxy hydroquinone, benzoquinone), and finally the generation of muconic acid, and nitrogenous intermediates (4-aminophenol and acetamide) [40]. It is important to note that the catalyst can be reutilized up to 7 times without losing its photocatalytic effect. However, with the degradation percentages obtained for each pollutant, it can be deduced that a catalyst is an excellent option.

3.3 Kinetic parameters

Several studies affirm that the reaction rate depends fundamentally on the concentration of the reagent [41]. The phenomena occurring on the surface of a catalyst have an essential role in the efficiency of heterogeneous photocatalysis because all photocatalytic processes are surface. A vital factor is the adsorption of the subjected pollutant molecules on the catalyst surface, where powerful e/h pairs, hydroxyl radicals, and superoxides are produced. These reactive species have a short lifetime of a few nanoseconds and must react immediately after production [42-44].

Therefore, the rapid and high adsorbed molecules of the pollutant on the catalyst surface play a vital role in the degradation efficiency because it increases the probability of collision between the pollutant molecules and the catalyst surface. Consequently, this increases the reaction of the pollutant molecules with the previously mentioned reactive species before they are deactivated by participating in the secondary reactions. In a balanced adsorption/desorption process, the kinetics of a heterogeneous photodegradation process (reaction rate = r: mg/L min) can be interpreted by the Langmuir-Hinshelwood model [8, 35, 45]. Therefore, the rate photodegradation process can be studied by Equation 6, which is valid for a zero-order rate process. The experimental results show that the photocatalytic reaction follows first-order kinetics (Eq. 6).

$$r_a = \frac{dCa}{dt} = kC \qquad (6)$$

Where r_a is reaction rate, C is concentration, and k is the reaction constant.

The heterogeneous photodegradation processes have conditions in which both reactants and degradation products can absorb photons. Integration of Equation 6 results in the Hinshelwood equation (Eq. 7) for a pseudo-first-order reaction kinetics [46].

$$ln\frac{C}{C_0} = -k_{ap}t \qquad (7)$$

Where, $\frac{C}{C_0}$ is the normalized concentration, t is the time, and k_{ap} is the constant of the reaction apparent.

In **Fig. 8** and **9**, the logarithms of the normalized concentrations $\frac{C}{C_0}$ were plotted as a function of reaction time (Eq. 8); the values of the apparent reaction constant were obtained by linear regression.

$$C = Co + e^{-k_{ap}t} \qquad (8)$$

With the above graphs, the values of the apparent reaction constant for each concentration were obtained; with these data, the results obtained in **Table 3** and **Table 4** were calculated, showing the numerical values of the reaction rate of acetaminophen and pyridine, respectively.

As indicated by the above results, the reaction rate constant decreases with an increasing initial concentration of the reagent, which means that the higher the concentration, the slower the degradation, and therefore the total conversion is achieved in a long time.

The initial concentration dependence of the photodegradation of acetaminophen and pyridine is explained by the fact that the degradation reaction takes place on the surface of the catalyst where the .OH radicals, generated by the action of UV light, are located.

When the concentration of contaminants is high, inadequeate .OH radicals are produced because the organic molecules are adsorbed on the catalyst particles. Therefore, the contaminants to be degraded are always present [35]. This indicates that photocatalytic oxidation reactions follow Langmuir-Hinshelwood kinetics (Eq. 9) [47].

$$-r_a = -\frac{dC}{dt} = \frac{k_1 C}{1 + k_2 C + \sum k_i C_i} \qquad (9)$$

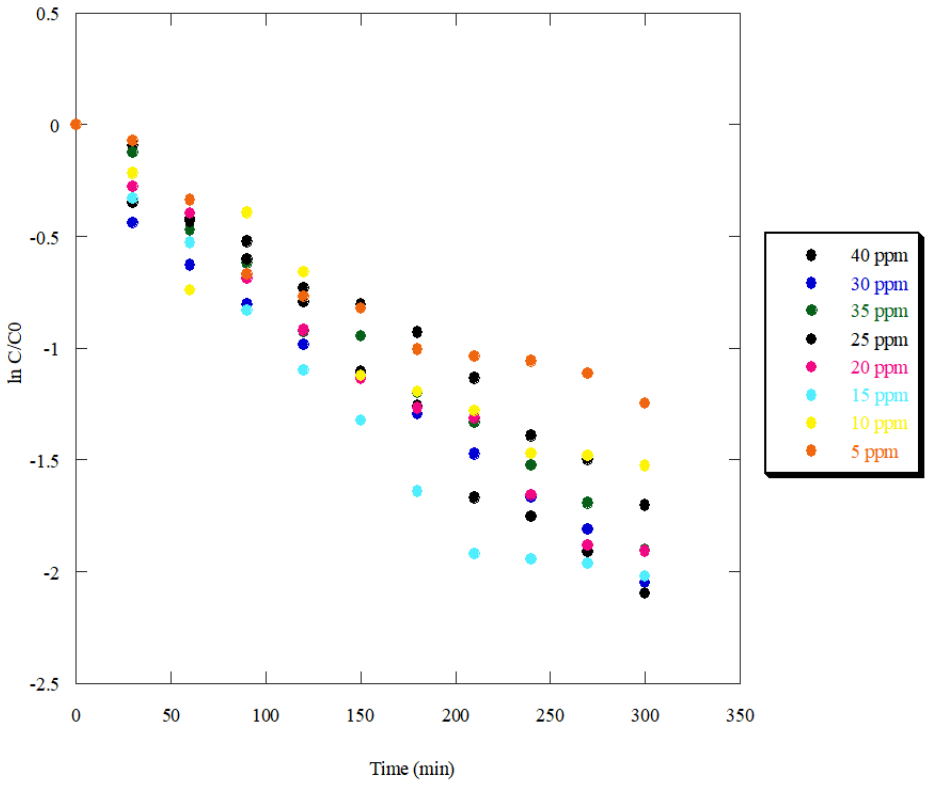

Fig. 8 Kinetics of acetaminophen reaction using Al-TiO_2/ Al_2O_3 (catalysts dose: 11.6 g L^{-1}, photodegradation time: 300 min, pH: 6.8)

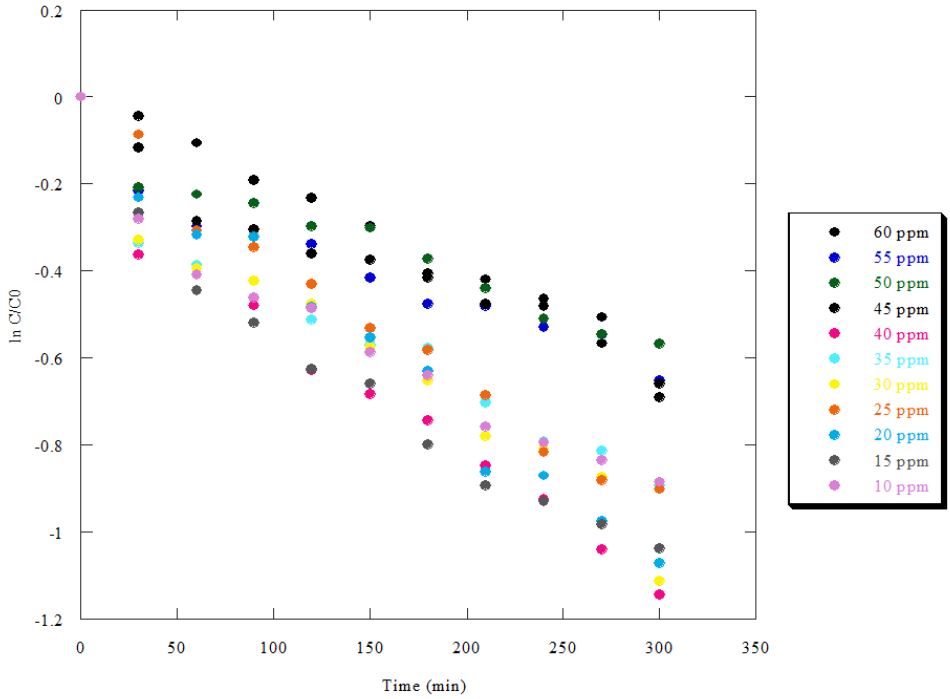

Fig. 9 Kinetics of pyridine reaction using Al-TiO_2/ Al_2O_3 (catalysts dose: 11.6 g L^{-1}, photodegradation time: 300 min, pH: 6.8)

Table 3 Numerical values of the reaction rate for acetaminophen

$C=C_0$	K_{ap}	R^2	$r_{a\ t=0}$ (ppm/h)	$1/r_a$(h/ppm)	$1/C_0$ (1/ppm)
5	0.0041	0.9131	0.0205	48.78049	0.2
10	0.0052	0.9107	0.052	19.23077	0.1
15	0.0072	0.9523	0.108	9.259259	0.066667
20	0.0065	0.9867	0.13	7.692308	0.05
25	0.0071	0.9891	0.1775	5.633803	0.04
30	0.0062	0.9862	0.186	5.376344	0.033333
35	0.0063	0.9903	0.2205	4.535147	0.028571
40	0.0056	0.9907	0.224	4.464286	0.025

Table 4 Numerical values of the reaction rate for pyridine

$C=C_0$	K_{ap}	R_2	$r_{a,\ t=0}$(ppm/h)	$1/r_a$(h/ppm)	$1/C_0$(1/ppm)
10	0.0026	0.9328	0.026	38.46154	0.1
15	0.0032	0.9412	0.048	20.83333	0.066667
20	0.0034	0.9803	0.068	14.70588	0.05
25	0.003	0.9808	0.075	13.33333	0.04
30	0.003	0.9465	0.09	11.11111	0.033333
35	0.0025	0.9212	0.0875	11.42857	0.028571
40	0.0033	0.9586	0.132	7.575758	0.025
45	0.0018	0.9121	0.081	12.34568	0.022222
50	0.0017	0.9432	0.085	11.76471	0.02

Where r_a is reaction rate, C is concentration, k_1,k_2 is reaction constant and adsorption constant respectively, and $\sum k_i C_i$ represents the adsorption term of all intermediate products of the photodegradation reaction of organic compounds.

If experimental data are analyzed at very short reaction times, it is possible to disregard the term adsorption of intermediate products. Then the (Eq. 9) becomes the (Eq.10) [35].

$$-r_a = -\frac{dc}{dt} = \frac{k_1 C}{1+ k_2 C} \qquad (10)$$

Now, if we analyze (Eq.10) for very low concentrations of acetaminophen where $k_2 C \ll 1$ we obtain equation 11.

$$-r_a = -\frac{dC}{dt} = \frac{k_1 C}{1+ k_2 C} = \frac{k_1 C}{1} = k_1 C \qquad (11)$$

$$-r_a = -\frac{dC}{dt} k_1 \qquad (12)$$

As can be seen (Eq. 12) is a combination of the first-order velocity with kinetic coefficient k_1. For high concentrations $k_2 C \ll 1$, (Eq. 13) is obtained.

$$-r_a = -\frac{dC}{dt} = \frac{k_1 C}{1 + k_2 C} = \frac{k_1 C}{k_2 C} = \frac{k_1}{k_2} \qquad (13)$$

$$-r_a = -\frac{dC}{dt} = \frac{k_1}{k_2} \qquad (14)$$

Where, (Eq. 14) is an equation of the velocity of zero-order, with kinetic coefficients $k_1 and\ k_2$. Based on the above analysis, it can be shown that the general kinetic form can be represented as follows (Eq.15):

$$-r_a = -\frac{dC}{dt} = \frac{k_1 C^m}{1 + k_2 C^n} \qquad (15)$$

If the exponents m and n have a value of 1, the constants k_1 and k_2 can be determined directly from the reaction rate graph concerning the concentration. The (Eq. 15)

can be linearized using the following initial conditions; t=0, C=C0. The initial reaction rate equation (Eq.15) is transformed into its inverse (Eq.18) where the ordered source is k_2/k_1 and the slope is given by $1/k_1$.

$$-r_{a|t=0} = \frac{k_1 C_0}{1 + k_2 C_0} \quad (16)$$

$$\frac{1}{-r_{a|t=0}} = \frac{1 + k_2 C_0}{k_1 C_0} = \frac{1}{k_1 C_0} = \frac{k_2 C_0}{k_1 C_0} \quad (17)$$

$$\frac{1}{-r_{a|t=0}} = \frac{1}{k_1 C_0} = \frac{k_2}{k_1} \quad (18)$$

Once the corresponding equations were obtained, the initial reaction rate was determined from the experimental data of concentration versus time for each test (for each pollutant). This was done by multiplying the reaction constant (k_{ap}) by the initial concentration (C_0). The results are shown below by plotting ($1/-r_a$) vs ($1/C_0$) as shown in **Fig. 10**, and **11**, which correspond to the data shown in **Tables 2** and **3** according to (Eq 16).

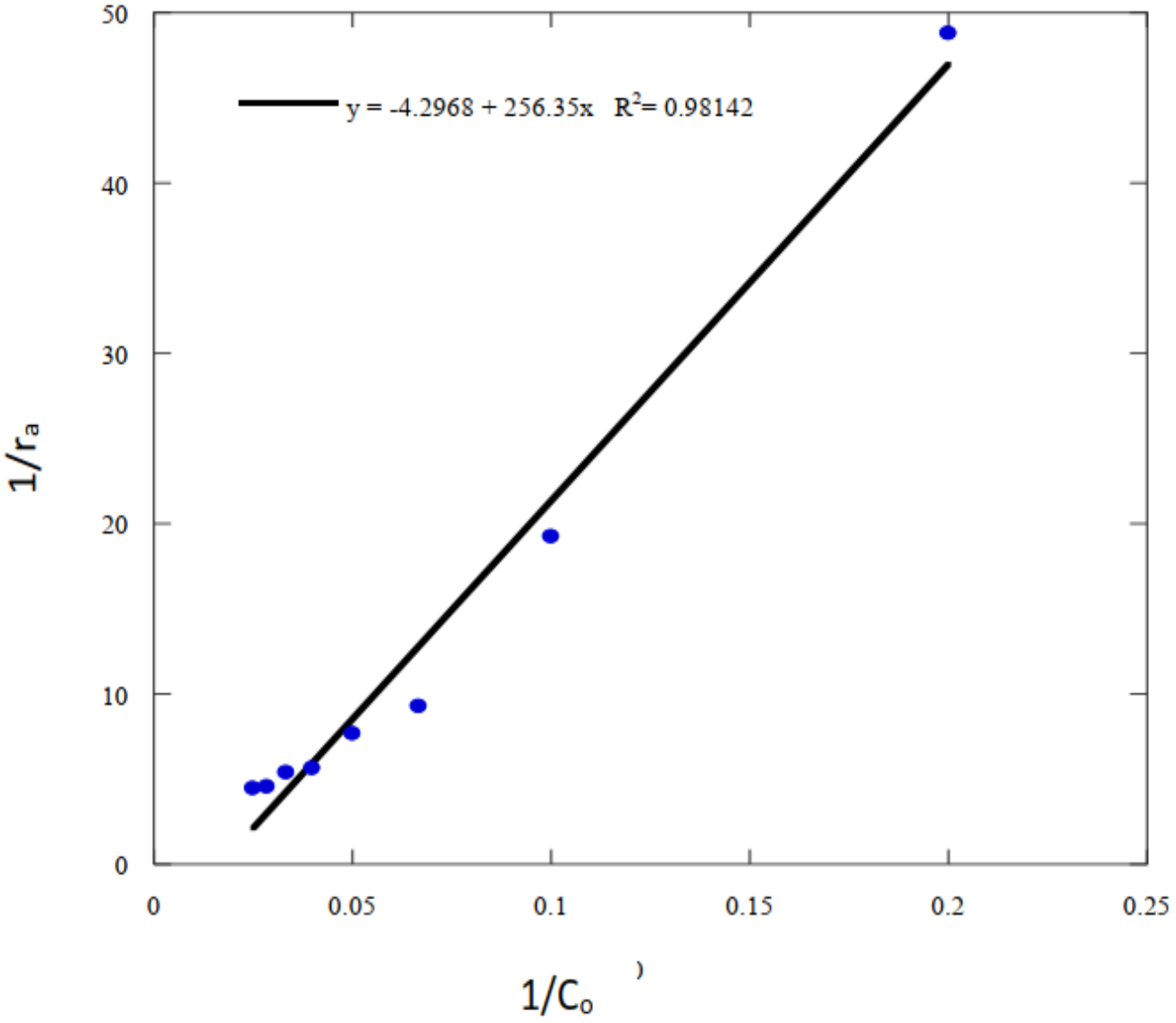

Fig. 10 Typical Langmuir- Hinshelwood plots obtained from the photodegraded acetaminophen (catalysts dose: 11.6 g L^{-1}, photodegradation time: 300 min, pH: 6.8).

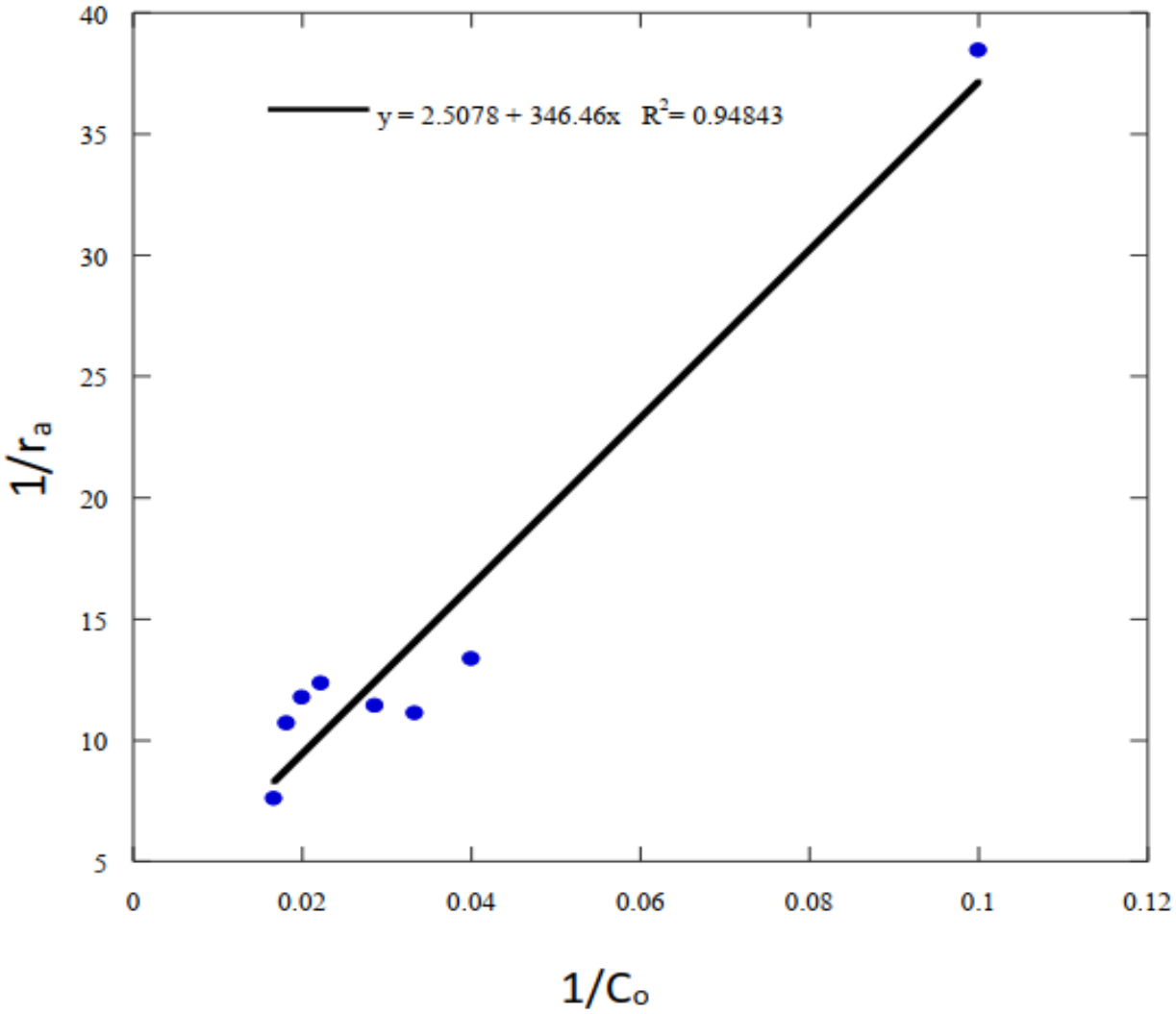

Fig. 11 Typical Langmuir- Hinshelwood plots obtained from the photodegraded pyridine (catalysts dose: 11.6 g L^{-1}, photodegradation time: 300 min, pH: 6.8).

The result obtained of R^2= 0. 9484 for pyridine presented in **Fig. 11** gives us a clear idea of how the points are distributed within the graph, understanding that the ideal value for R^2=1 where all the points would be positioned on the line. In the case of **Fig. 10**, the values are very close to the line, which gives a value of R^2= 0.9814. After evaluating the constants, **Table 5** is obtained.

Where k_1 represents the reaction constant and k_2 the adsorption constant, it can be observed that these reactions have a first-order behavior at low concentrations and pseudo-first-order or zero-order at higher concentrations, which confirms the behavior of the Langmuir-Hinshelwood model represented in **Fig. 12** corresponding to the Langmuir-Hinshelwood model for acetaminophen and **Fig. 13** to the Langmuir-Hinshelwood model for pyridine.

In this research, the degradation was realized with TiO_2 doped with aluminum. **Table 5** compares the degradation percentages obtained by other authors who used undoped TiO_2 [34, 35], showing that the removal of contaminants is lower than those obtained with TiO_2 doped with other metals. The results indicate that the catalytic properties of TiO_2 improve when combined with aluminum or any other metal. As observed in **Table 6**, the catalyst improves its photocatalytic power if it is combined with more than one metal. Considering that the operating cost would increase when using more than one metal in the catalyst, synthesis is imperative.

Table 5 Values of the k_1 and k_2 constants for the contaminant's acetaminophen and pyridine

Values of k_1 and k_2 for acetaminophen	Values of k_1 y k_2 for pyridine
k_1 =0.390092 min^{-1}	k_1 = 0.00308938 min^{-1}
k_2 =0.01676146$(\frac{ppm}{L})^{-1}$	k_2 = 0.00664926 $(\frac{ppm}{L})^{-1}$

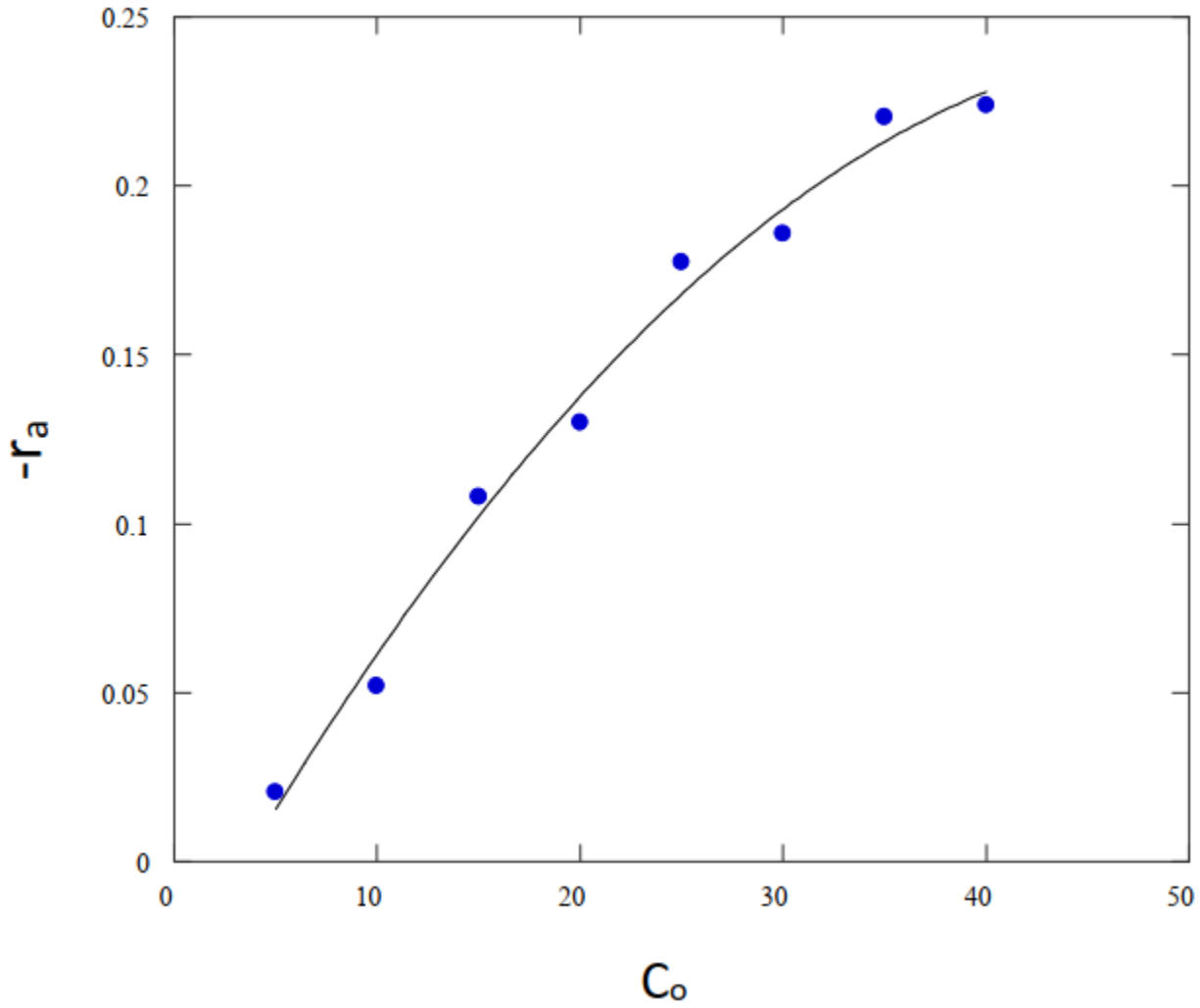

Fig. 12 Graphical representation of the Langmuir-Hinshelwood model evaluation for acetaminophen (catalysts dose: 11.6 g L^{-1}, photodegradation time: 300 min, pH: 6.8)

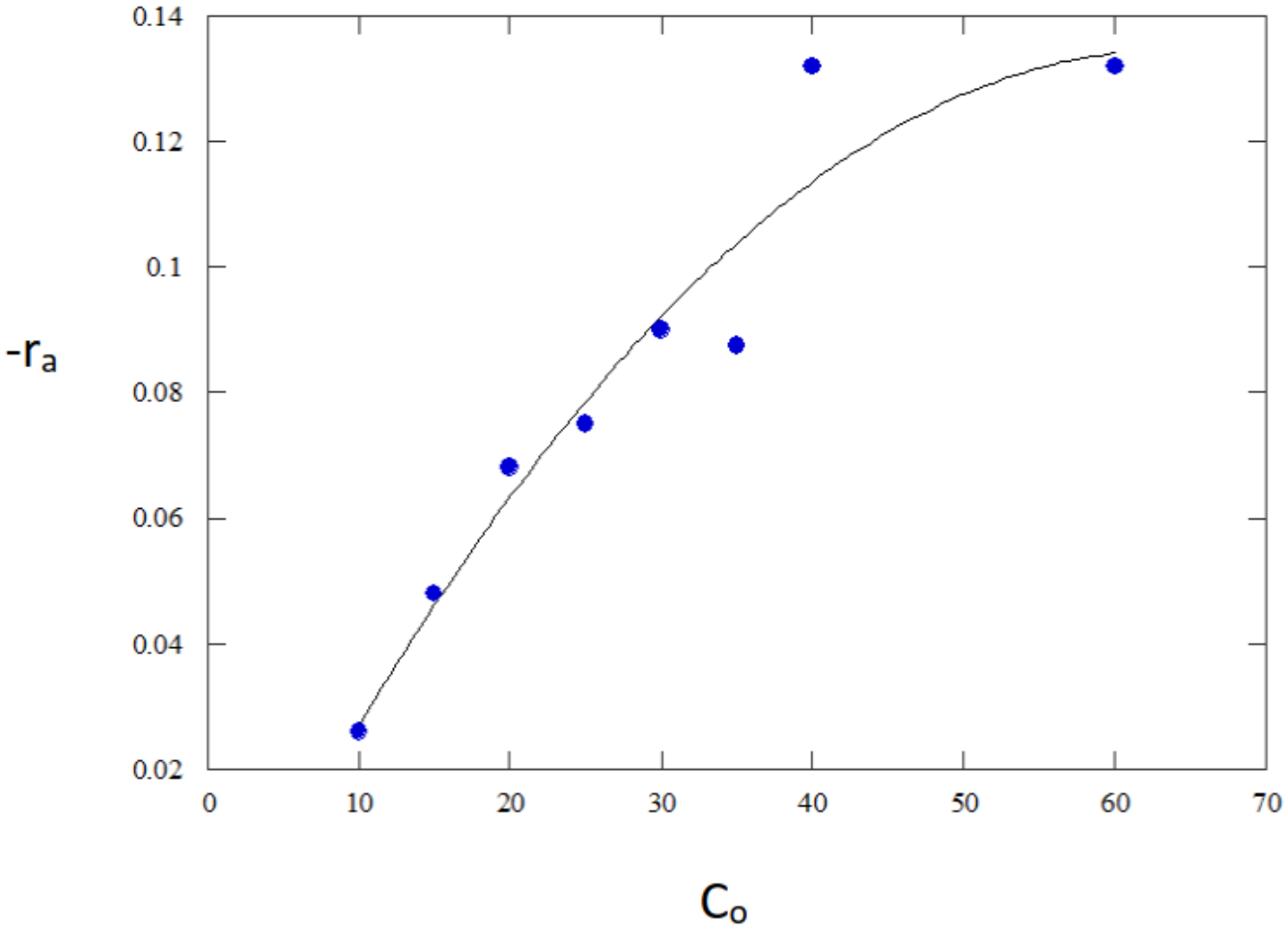

Fig. 13 Graphical representation of the Langmuir-Hinshelwood model evaluation for pyridine (catalysts dose: 11.6 g L^{-1}, photodegradation time: 300 min, pH: 6.8)

Table 6 Comparison table of the photocatalytic degradation

Catalyst	Description	Time (min)	Degradation (%)	References
TiO_2	Vinasses (phenol)	4320	82.39	[14]
TiO_2	Methylene blue	195	47	[48]
TiO_2	Toluene	120	62	[49]
TiO_2/SC	Methylene blue	120	97.19	[50]
$Cu_2O/WO_3/TiO_2$	Acetaminophen	60	92.5	[51]
TiO_2 (TAB)-ZnO	Methylene blue	180	97	[52]
Al-TiO_2	Acetaminophen	300	85	[Present work]
Al-TiO_2	Pyridine	300	70	[Present work]

The percentage of pollutant degradation increases using modified TiO_2 due to electron transfer concerning the reduced recombination of electron-hole pair charge carriers in the multiphase nanostructure. Adsorption of both oxidant and pollutant is a fundamental parameter in a heterogeneous photodegradation process [48].

The results obtained in the present study are in good agreement with earlier reports (**Table 7**) [49-52]; it was

Table 7 Comparison table of the rate constant (K_{app})

Catalyst	Rate constant K_{app} (min^{-1})	References
TiO_2	0.009	[14]
TiO_2	0.005	[39]
TiO_2	0.006	[39]
TiO_2	0.0180	[45]
TiO_2	0.0034	[48]
Al-TiO_2	0.0056, 0.0033	[Present work]

observed that the results corresponding to the apparent constant obtained for acetaminophen using the doped catalyst are higher in comparison with other authors [30, 52]. It is worth mentioning that the difference between apparent constants is due to several factors such as the concentration of the pollutant, the type of pollutant, temperature of the photocatalytic process, pH, and removal time.

One of the reasons for the lack of total contaminant removal could have been the size of the catalyst crystals, since with increasing crystal size, the rate constant decreases. It has been proved that the degradation process is more significant for smaller crystal sizes, so the result of the degradation of pyridine and acetaminophen could have been affected by the nature and crystal size of the titanium dioxide nanoparticles with aluminum. So, it is advisable to control the nanocrystal synthesis to obtain smaller crystal sizes and observe the catalyst's photocatalytic power as other authors have done [45].

Another reason that could interfere with the total removal of the contaminant is the formation of the intermediate products of the contaminant degradation that could resist during 300 min of removal; therefore, a long time may be required for the total mineralization of the pollutant [46]. However, according to the results obtained, it could be proved that the synthesized catalyst can serve as an effective catalyst to degrade not only pyridine and acetaminophen but also any other emerging compound discharged in wastewater.

4. Conclusions

An Al-TiO_2/ Al_2O_3 catalyst was synthesized to degrade acetaminophen and pyridine under UV irradiation. The results of the XDR characterization of the catalyst showed the presence of the anatase and rutile phases, without traces of impurities or unwanted contaminants, presenting a behavior like that of commercial oxides, with a particle size of 50 nm. TEM results revealed that the semiconductor particles are uniformly distributed on the support favors solid-liquid contact. EDS analysis shows the ratio of the semiconductor to the dopant favored photon collection upon semiconductor activation. The removal efficiency was 85 % and 70 % for acetaminophen and pyridine, respectively, obtaining better results for acetaminophen because the initial concentration of the contaminant was lower than that used for pyridine, demonstrating that the concentration of the contaminant has an essential role in obtaining higher removal percentages. Another reason could be the detachment of the doped catalyst from the support due to its use and washing in each degradation test. The results showed that the kinetics of degradation of paracetamol and pyridine behave according to the kinetic model of the Langmuir-Hinshelwood equation. The synthesized catalyst can be reused up to 7 times with high efficiency, proving that this system is feasible for degrading recalcitrant emerging compounds. The synthesized catalyst can be reused up to 7 times with high efficiency by degrading organic compounds at low and high concentrations, obtaining a removal efficiency of up to 85 % of acetaminophen and 70 % for pyridine after 300 minutes of reaction. The behavior of the reactions for the different photocatalysts was determined using the LH- HW model. It was observed that alumina beads are a good option as a support for the photocatalyst as they are highly porous, which allows a good distribution of titanium oxide on alumina. This system is viable for degrading compounds with high and low concentrations of recalcitrant emerging compounds such as acetaminophen and pyridine.

Acknowledgments

Special thanks are due to the Ph.D. Aida Luz Villa Holguín from the University of Antioquia, Medellin, Colombia, for the attention given to the development of the characterization of the catalyst.

References

[1] M. Rajput, B. Mishra, Biocatal. Agric. Biotechnol. 17 (2019) 32-35.
[2] V. Bernal, L. Giraldo, P. J. Moreno, Rev. Colomb. Quim. 47 (2018) 54-62.
[3] EPA. United States Environmental Protection Agency: Paracetamol.(2021). https://sor.epa.gov/sor_internet/registry/substreg/searchandretrieve/advancedsearch/externalSearch.do?p_type=CASNO&p_value=103-90-2#.

[4] U.S. Food and Drug Administration. Acetaminophen Information. (2017). https://www.fda.gov/drugs/information-drug-class/acetaminophen-information. Revised March 5, 2021.
[5] C. Tejada, E. Quiñonez, M. Peña, Revista Facultad de ciencias básicas. 10 (2014) 80-101.
[6] Z.V. Robledo, M. M. Velázquez, S. J. Montañez, E. J. Pimentel, C. A. Vallejo, C. M. López, G. J. Venegas, Rev. Int. Contam. Ambient. 33 (2017) 221-235.
[7] O. A. Zalat, M. A. Elsayed, J. Environ. Chem. Eng. 1 (2013) 137-143
[8] E. Leyva, C. Montalvo, E. Moctezuma, S. Leyva. J. Ceramic Process. Res. 9 (2008) 455-462.
[9] Q. Lu, C. Zhang, W. Wang, B. Yuan, Y. Zhang, B. Rittmann. Sci. Total Environ. 654 (2019) 473-479.
[10] H. Vo, G. Le, T. Niguyen, T. Buin, X. Niguyen, E. Rene, T. Vo, N. Cao, R. Mohan, Chem. 236 (2019)124-134
[11] V. Gosu, P. Sikarwar, V. Subbaramaiah, J. Environ. Chem. Engin. 6 (2018) 1000-1007.
[12] L. Chu, S. Yu, J. Wang, Radiat. Phys. Chem. 144 (2018) 322-328.
[13] S. Malato, L. P. Fernández, M. I. Maldonado, J. Blanco, W. Gernjak, Catal. Today. 147 (2009) 1-59.
[14] P. R. Gines, R.E. Oropeza, R. C. Montalvo, L. D. Cantú, Rev. Mex. Ing. Quim. 19 (2020) 653-665.
[15] R. Camposeco, S. Castillo, G.V. Rodríguez, R. M. Hinojosa, A.I. Medina, C. I. Mejia, J. Photochem. Photobiol. A. 353 (2018) 114-121.
[16] L. F. Garces, M. L. Hernadez, Gest. Ambient 16 (2008) 1-12.
[17] S. Sajjadifar, I. Amini, M. Karimian. Iran. J. Catal., 11 (2021) 59-67.
[18] H. Pouretedal, M. Fallahgar, F. Pourhasan, M. Nasiri. Iran. J. Catal., 7, (2017) 317-326.
[19] H. Derikvandi, M. Vosough, A. Nezamzadeh-Ejhieh, Environ. Sci. Pollution Res. 27 (2020) 27582–27597.
[20] H. Derikvandi, M. Vosough, A. Nezamzadeh-Ejhieh, Inter. J. Hydrogen Energy. 46 (2021) 2049-2064.
[21] T. Zhang, M. Xu, J. Li, Catal. Today. 376 (2021) 162–167.
[22] S. I. Ahmad, H. Hamoudi, J. Ponraj, K. M. Youssef, Carbon. 178 (2021) 657-665.
[23] A. Ziashahabi, R. Poursalehi, Procedia Materials Sci. 11 (2015) 434-437.
[24] S. Sakthivel, M.V. Shankar, M. Palanichamy, B. Arabindoo, V. Murugesan, J. Photochem. Photobio. A: Chem. 148 (2002) 153–159.
[25] L. Lecheng, P.C. Hiu, H. Xijun, Y. Po-Lock, Ind. Eng. Chem. Res. 38 (1999) 3381-3385.
[26] S. Hira, H. Hui, M. Yusuf, K. Park, Catal. Commun. 141 (2020) 1-11.
[27] E. Mosquera, N. Rosas, A. Debut, V.H. Guerrero, Rev. Politécnica. 36 (2015) 7-14.
[28] D. Wodka, E. Bielanska, R. Socha, M. Elzbieciak, J. Gurgul, P. Nowak, P. Warszynki, O. Kumariki, Appl. Mater. Interfaces. 2 (2010) 1945-1953.
[29] V. Subramanian, E. Wolf, P. Kamat, Am. Chem. Soc. 126 (2004) 4943–4950.
[30] C. Aguilar, C. Montalvo, B. Zermeño, R. Cerón, J. Cerón, F. Anguebes, M. Ramírez, Int. J. Environ. Sci. Technol. 16 (2019) 843–852.
[31] V. Loddo, M. Bellardita, G. Camera, F. Parrino, L. Palmisano, Advanced Oxidation Process. In Current Trends and Future Developments on (Bio-) Membranes; Elsevier: Palermo, Italy, 2018.
[32] H. Calderón, Rev. Interdis. Nanocien. Nanotecn. 13 (2020) 133-156.
[33] M. A. Vargas, Y.H. Ochoa, Y. Ortegón, P. Mosquera, J. E. Rodríguez, R. J. Camargo, Ing. Desarrollo. 29 (2011) 186-201.
[34] Y. Ochoa, Y. Ortegón, P.J. Rodríguez, Rev. Fac. Ing. Univ. Antioquia. 2010 (2010) 29-40
[35] E. Moctezuma, H. Zamarripa, E. Leyva, Rev. Int. Contam. Ambient. 19 (2003) 117-125
[36] C. Fotiadis, N.P. Xekoukoulotakis, D. Mantzavinos, Catal. Today. 124 (2007) 247–253.
[37] S. Senobari, A. Nezamzadeh, Spectroch. Acta Part A: Mol. Bio. Spectros. 196 (2018) 334–343.
[38] A. Nezamzadeh, Z. Salimi, Desalination. 280 (2011) 281–287.
[39] A. Kumar and G. Pandey, Mat. Sci. Ing. Inter. J. 1 (2017) 106-114.
[40] S. Ege, Química orgánica. Estructura y reactividad. First ed., Reverté, México, 2000.
[41] M. Mehrali-Afjania, A. Nezamzadeh, H. Aghaei, Chem. Phys. Lett. 759 (2020) 137873-137889.
[42] A. Nezamzadeh, M. Khorsandi, J. Hazard. Mater. 176 (2010) 629–637.
[43] N. Arabpour, A. Nezamzadeh-Ejhieh, Mater. Sci. Semicond. Proces. 31 (2015) 684–692.
[44] A. Yousefi, A. Nezamzadeh-Ejhieh, Irán. J. Catal. 11 (2021) 247-259.
[45] B. Manikandan, K. R. Murali and R. John, Irán. J. Catal. 11 (2021) 1-11.
[46] S. Salmanderis, A. Nezamzadeh, Desal. Water Treat. 197 (2020) 200-212.
[47] H. S. Fogler, Elements of Chemical Reaction Engineering, second ed., Prentice-Hall, 2000.
[48] R. S. Dassanayake, E. Rajakaruna, N. Abidi, J. Appl. Polym. Sci. 135 (2017) 45908-45922.

[49] Y. Zeng, Y. Zhan, R. Xie, K. Hu, J. Cao, D. Lei, B. Liu, M. He, H. Huang, Chemosphere. 244 (2020) 12567-12579.
[50] Y. Zhai, W. Feng, Q. Wang, X. Ning, Catal. Commun. 58 (2015) 103–107.
[51] J. Chau, C. Lai, B. Leo, J. Juan, M. Johan, Catal. Commun. 163 (2022) 384-396.
[52] B. Manikandan, R. John, Iran, J. Catal. 10 (2020) 1-16.